CHEMISTRY OF MATERIALS
Cite This: Chem. Mater. 2018, 30, 7280−7286
Article
pubs.acs.org/cm

Strategies for Localizing Multiple Functional Groups in Mesoporous Silica Particles through a One-Pot Synthesis

Nicola Zucchetto and Dominik Brühwiler*

Institute of Chemistry and Biotechnology, Zürich University of Applied Sciences (ZHAW), CH-8820 Wädenswil, Switzerland

Supporting Information

ABSTRACT: The process of postcondensation for the functionalization of mesoporous silica is based on the cooperation between the end-on growth of arrays of silica nanochannels and the steric hindrance of the functional silanes (R-silanes). To obtain particles with differently functionalized surfaces (thiol and amino groups), the delayed addition of another R-silane was introduced. This tandem postcondensation approach allows for three selective functionalization strategies, depending on the mobility and the steric hindrance of the R-silanes. Following these one-pot synthesis strategies, functional groups can be placed independently on the pore entrances and on the internal surface of the mesoporous silica particles. Confocal laser scanning microscopy was used to image the functional group distribution after selective coupling with a fluorescent dye. Nitrogen sorption measurements were conducted to confirm the well-defined mesoporosity of the functionalized products.

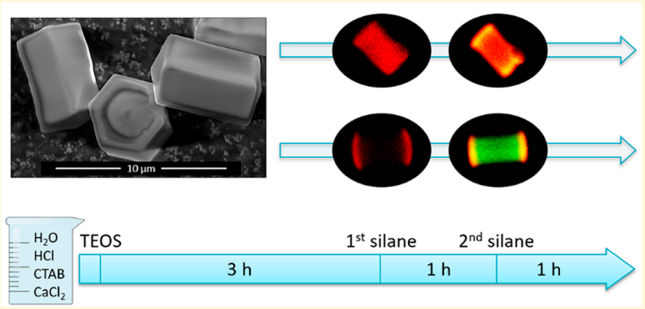

INTRODUCTION

Synthesis, customization, and application of mesoporous silica materials has been a topic of interest since their discovery in 1992.[1] The scientific ubiquity of these materials is due to the convenient particle design in terms of size, morphology, and functionalization. Morphology and size are well-studied aspects, particularly in view of potential applications in the field of drug delivery, where these two parameters determine the biodistribution of the particles.[2,3]

A key characteristic of mesoporous silica materials is the possibility to functionalize the surfaces with a wide variety of organic compounds.[4] The introduction of active moieties leads to versatile and unique functional particles. A wide array of applications is possible with these functional mesoporous materials such as drug delivery,[5−7] catalysis,[8] sensing,[9−11] adsorption,[12,13] and chromatography.[14] Postsynthetic treatments[15,16] and co-condensation[15−17] are the approaches generally used for achieving surface functionalization. Recently, alternative methods have been proposed to obtain a specific localization of the functional moieties. Core−shell mesoporous silica nanoparticles were obtained via a modified co-condensation process, adding the functional silanes (R-silanes) consecutively at the beginning (core) and during the reaction (shell).[18] Postcondensation of arrays of silica nanochannels (ASNCs)[19] allows for the functionalization of different particle surfaces in a one-pot reaction preserving the characteristic hexagonal morphology and the porous properties of the material. ASNCs are hexagonal prismatic mesoporous silica particles (Figure 1) characterized by a one-dimensional channel system with three inherently different surface regions:

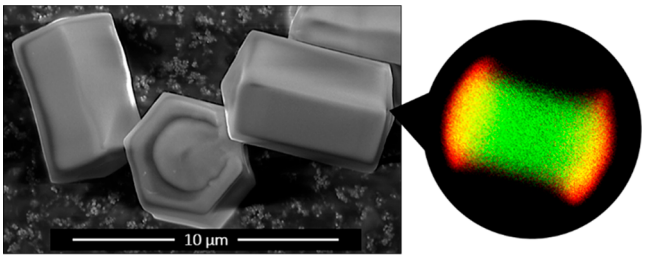

Figure 1. Scanning electron microscopy (SEM) image of ASNCs and confocal laser scanning microscopy (CLSM) image showing an optical slice through the center of a bifunctionalized particle. The functionalized areas are pore entrances (red), internal (pore) surface (green), and the region between the internal surface and the pore entrances (yellow). The depicted sample features rhodamine-labeled amino groups at the pore entrances and uniformly distributed fluorescein-labeled thiol groups.

pore entrances (hexagonal faces), external surfaces (rectangular faces), and internal surfaces (cylindrical pores).[19]

It is instructive to compare ASNCs to hexagonal zeolites with one-dimensional channel systems, such as zeolite L. The latter can be considered the microporous crystalline counterpart of ASNCs. The selective functionalization of the pore entrances of zeolite L has been achieved postsynthetically by means of so-called stopcock molecules, which effectively seal the zeolite channels.[20,21] The resulting materials are of interest

Received: August 24, 2018
Revised: October 1, 2018
Published: October 12, 2018

DOI: 10.1021/acs.chemmater.8b03603
Chem. Mater. 2018, 30, 7280−7286

for the development of photonic devices.[22,23] However, because of the much larger pore size, the stopcock approach employed for zeolites cannot be readily adopted for mesoporous materials.

In contrast to spherical particles, where the growth is isotropic, ASNCs exhibit anisotropic growth. The predominant process in the growth of ASNCs occurs end-on, that is, at the pore entrances. Side-on growth is slower and increases the particle diameter.[24] The postcondensation strategy is based on the interplay between the end-on growth and the steric hindrance of the added R-silanes.[19] These two effects were used as driving forces to achieve a selective surface functionalization. The process of postcondensation was further developed to obtain multifunctionalized ASNCs. This advanced method, which we have termed tandem postcondensation, is based on the addition of different R-silanes (Figure 2) at two separate times during the ASNCs synthesis.

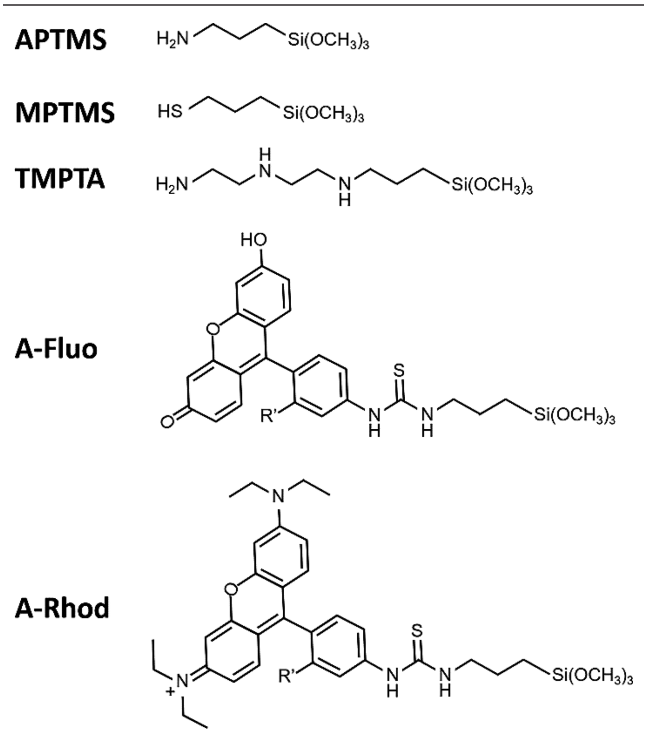

Figure 2. Structures and abbreviations of R-silanes (top three) and dye silanes (R′ = COOH).

The distribution of the functional groups was analyzed by means of CLSM after selective coupling between the functional moieties and fluorescent dyes.[19,25]

EXPERIMENTAL SECTION

Materials. Hexadecyltrimethylammonium bromide (CTAB, > 96%), calcium chloride ($CaCl_2$, ≥ 97%), concentrated hydrochloric acid (HCl, 37%), ammonium nitrate (≥98%), tetraethoxysilane (TEOS, 99.999%), 3-aminopropyltrimethoxysilane (APTMS, 99%), N^1-(3-trimethoxysilylpropyl)diethylenetriamine (TMPTA, technical grade), 3-mercaptopropyltrimethoxysilane (MPTMS, 95%), fluorescein isothiocyanate (FITC, isomer I, ≥ 90%), fluorescein diacetate 5-maleimide (Fd5M, suitable for fluorescence), rhodamine B isothiocyanate (RhITC, mixed isomers), and the solvents ethanol (pure, ≥ 99.8%), acetone (≥99.5%), and dimethylformamide (DMF, anhydrous, 99.8%) were obtained from Sigma-Aldrich.

Recrystallization of CTAB. Impurities in CTAB can affect the uniformity of the hexagonal prismatic morphology of the ASNCs. To ensure maximum reproducibility, recrystallization of CTAB is recommended. CTAB was recrystallized by dispersing an amount of 15 g in acetone (90 mL). The dispersion was heated to 50 °C under stirring and ethanol (30 mL) was added. After a few minutes, the clear solution was cooled to room temperature. After 1 h the precipitate was filtered and washed with acetone (30 mL) and the powder was dried in an oven at 80 °C.

Synthesis of Dye Silanes. The isothiocyanate dye (0.009 mmol, FITC or RhITC) was dissolved in ethanol (1 mL) and stirred for 5 min. APTMS (0.09 mmol) was added under stirring. The solution was degassed under vacuum, flushed with nitrogen several times, and kept under inert conditions. After they were stirred for 16 h at room temperature, the dye silane (A-Fluo and A-Rhod) solutions were used for the postcondensation reactions.

Synthesis of Functionalized ASNCs by Postcondensation and Tandem Postcondensation. Recrystallized CTAB (4.0 g, 11 mmol) and $CaCl_2$ (1.50 g, 13.5 mmol) were dissolved in a mixture of distilled H_2O (82 mL, 4.6 mol) and concentrated HCl (37%, 52 mL, 0.63 mol) by stirring for 15 min in a polypropylene beaker. The solution was subsequently cooled in an ice bath for 15 min under quiescent conditions, followed by the slow addition of cold TEOS (2.0 mL, 9 mmol) and further stirring for 30 s. The resulting mixture was kept at 0 °C under quiescent conditions for 3 h. After this period, the solution was stirred for 1 min while adding the R-silane or dye silane (first addition) and subsequently kept at 0 °C under quiescent conditions for 1 h. For tandem reactions the addition was repeated using a different functional silane (stirring for 1 min, adding the second R-silane or dye silane, and keeping the temperature at 0 °C for 1 h). The product was filtered and dried at 80 °C.

The amount of R-silane was calculated using an R-silane/TEOS molar ratio of 0.10 while the dye silane amount was calculated using a dye silane/TEOS molar ratio of 0.01.

For removal of the structure-directing agent, the product was first heated to 150 °C for 15 h (rate 1 °C min^{-1}) and then extracted by stirring 200 mg of the product in an ethanolic solution of ammonium nitrate (30 mL, 0.05 M) at 60 °C for 15 min, followed by centrifugation. After this extraction step was repeated twice, the product was washed with ethanol (30 mL) and dried at 80 °C overnight.

Fluorescent Labeling. The thiol-functionalized ASNCs were labeled by dispersing the dry powder (50 mg) in DMF (10 mL) and by adding Fd5M (3 mg). The dispersion was stirred overnight at room temperature, centrifuged, and washed once with DMF (10 mL) and twice with ethanol (20 mL). The samples were dried at 80 °C. The amino-functionalized ASNCs were labeled by dispersing the dry powder (50 mg) in absolute ethanol (10 mL) and by adding RhITC (3 mg). The dispersion was stirred overnight at room temperature, centrifuged, and washed with absolute ethanol until the washing solution became colorless. The samples were dried at 80 °C. Multifunctional ASNCs, containing both thiol and amino groups, were first coupled with Fd5M and subsequently with RhITC. This sequence was followed to prevent the nonselective coupling of the isothiocyanate dye. RhITC and Fd5M did not bind to pristine ASNCs.

The samples for CLSM were prepared by dispersing the labeled ASNCs (approximatively 1 mg) in ethanol (1 mL) and sonicating for 5 min. The dispersion was dropped on a microscope slide and dried in an oven at 80 °C.

Characterization. Scanning electron microscopy (SEM) images were obtained with a FEI Quanta FEG 250. CLSM was performed with an Olympus BX60 microscope equipped with a FluoView FV300 confocal unit and excitation at 488.0 and 543.5 nm (detection at λ < 530 nm for fluorescein and at λ > 570 nm for rhodamine). Nitrogen sorption isotherms (55 measurement points for adsorption and 40 points for desorption) were measured at 77 K with a Quantachrome Autosorb iQ MP. Pore size distributions and average pore diameters (d_{BJH} and d_{NLDFT}) were calculated by the BJH method[26] and by nonlocal density functional theory (NLDFT, silica with cylindrical pores, ASiQwin, version 3.01).[26,27] Surface areas S_{BET} were determined by multipoint BET.[28] Total pore volumes V_{tot} were

DOI: 10.1021/acs.chemmater.8b03603
Chem. Mater. 2018, 30, 7280−7286

derived from the amount of adsorbed nitrogen at a relative pressure of p/p_0 = 0.95. Adsorption isotherms were used for all calculations.

RESULTS AND DISCUSSION

Postcondensation with Bulky and Nonbulky Functional Silanes. In postcondensation, the steric hindrance of the functional silane and the anisotropic particle growth contribute to the selective surface functionalization.[19] To obtain additional information regarding the factors governing the distribution of the moieties on the particle surfaces, various functional silanes were used (Figure 2). The CLSM images of the postcondensed samples are reported in Figure 3. The

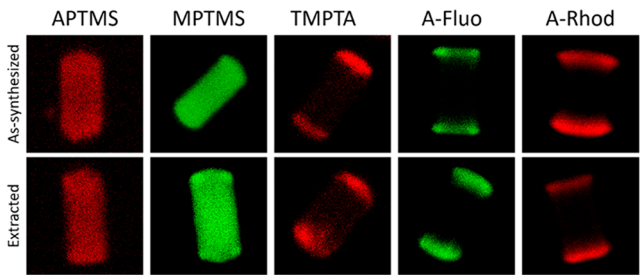

Figure 3. CLSM images of functionalized ASNCs synthesized by postcondensation before (top) and after (bottom) extraction of the structure-directing agent. The samples prepared with APTMS and TMPTA were coupled with RhITC (excitation at 543.5 nm), while the sample prepared with MPTMS was coupled with Fd5M (excitation at 488.0 nm). Representative optical slices in the middle of the particles were selected.

images represent the functional group distribution through an interior plane of the particle after dye coupling (RhITC for the samples prepared with APTMS or TMPTA, and Fd5M for the sample prepared with MPTMS). For the precoupled dye silanes (A-Fluo and A-Rhod) no further labeling step was necessary.

The CLSM images show two distinct trends regarding the functional group distribution. A uniform particle functionalization was obtained with the nonbulky APTMS and MPTMS because of their high mobility. The bulky TMPTA, A-Fluo, and A-Rhod, on the other hand, accumulated at the pore entrances as a consequence of the steric hindrance and preferential end-on growth. In contrast to the postsynthetic treatment of ASNCs with bulky alkoxysilanes, where the functionalization of the external surface is homogeneous,[25] postcondensation yields particles with only a negligible degree of lateral surface functionalization. This can be attributed to the comparatively slow side-on growth of the ASNCs.

Synthetic Strategies for Multifunctional Particles: Tandem Postcondensation. The basic principle of the postcondensation process is the addition of a functional silane after the characteristic particle morphology of the ASNCs is obtained. The anisotropic particle growth and the steric hindrance of the functional silane are the driving forces leading to a selective surface functionalization.[19] Tandem postcondensation employs a delayed secondary addition of a further functional silane. The particles thus obtained contain multiple moieties localized on different particle surface regions. The general scheme of tandem postcondensation and strategies using the consecutive addition of bulky and nonbulky functional silanes are reported in Figure 4. APTMS and MPTMS are thereby classified as nonbulky silanes because of their high mobility and their ability to uniformly functionalize the ASNCs. TMPTA and the dye silanes, A-Fluo and A-Rhod, are bulky silanes because of their tendency to postcondense on the hexagonal faces of the ASNCs. The samples are designated according to the sequence by which the silanes have been added to the reaction, for example, APTMS_MPTMS for a sample prepared by first adding APTMS and then MPTMS.

Tandem Postcondensation with Nonbulky Silanes (Case I). CLSM images of experiments conducted with APTMS and MPTMS are reported in Figure 5. As expected, the ASNCs were uniformly functionalized by the first silane as shown in panels B for APTMS_MPTMS (Figure 5, rhodamine coupled to amino groups) and in panels A for MPTMS_APTMS (Figure 5, fluorescein coupled to thiol groups). This uniform initial functional group distribution led to a localized condensation of the second silane, which accumulated at the pore entrances. These results are visible in Figure 5, panels A for APTMS_MPTMS (fluorescein coupled

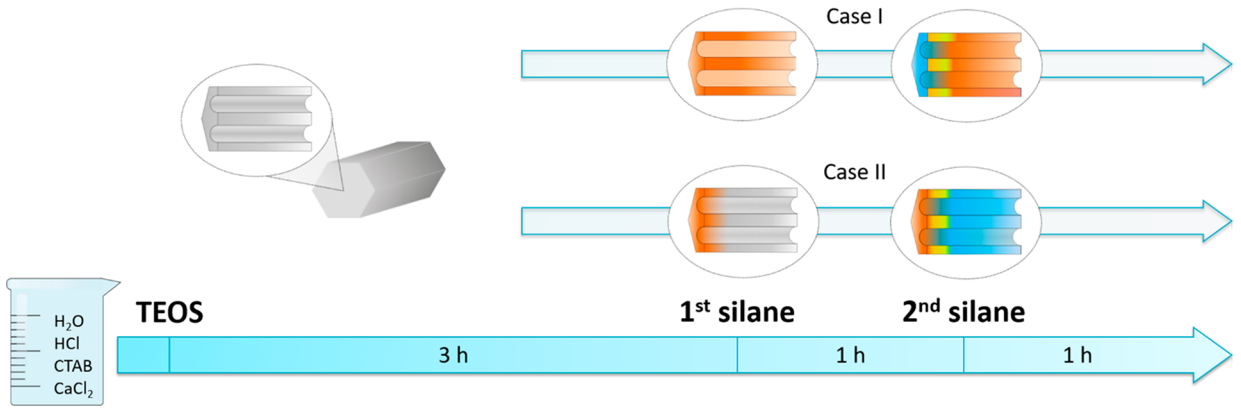

Figure 4. Reaction scheme of tandem postcondensation and selective functionalization strategies. When the ASNCs reach their typical hexagonal prismatic shape (3 h after the TEOS addition), the first functional silane is added (first silane). After a short period of reaction (1 h), addition of the second functional silane follows (second silane). The colored areas represent the different silanes and their corresponding location in the pores. The first silane is displayed in orange, while the second silane is blue. Overlapping functionalization is represented by the yellow regions. The outcome of the reaction in terms of the functional group distribution depends on the two types of silanes: case I was obtained when the first silane was nonbulky (APTMS or MPTMS). Case II was observed when the first silane was bulky (TMPTA). The reaction system with A-Fluo and A-Rhod also resulted in a case II distribution irrespective of the addition sequence.

DOI: 10.1021/acs.chemmater.8b03603
Chem. Mater. 2018, 30, 7280−7286

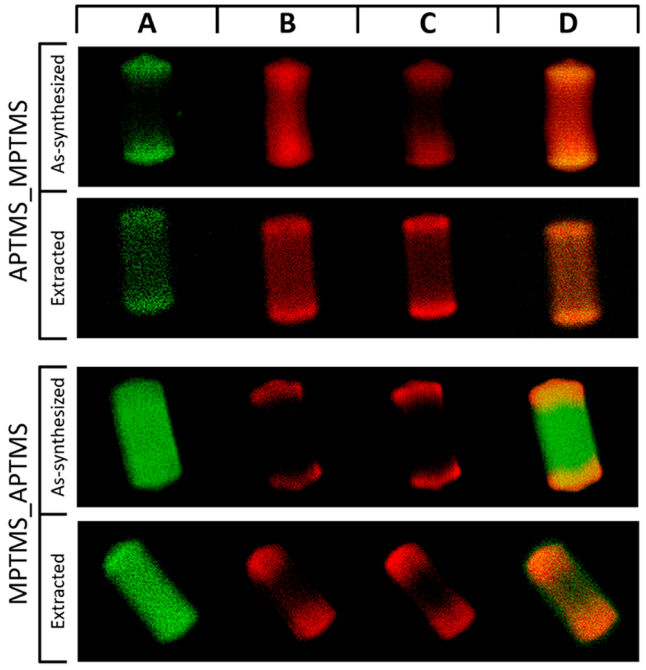

Figure 5. CLSM images of ASNCs prepared by tandem postcondensation. Top: APTMS and subsequent addition of MPTMS. Bottom: MPTMS and subsequent addition of APTMS. Excitation at 488.0 nm and observation of fluorescein fluorescence (panels A), excitation at 543.5 nm and observation of rhodamine fluorescence (panels B), excitation at 488.0 nm and observation of rhodamine fluorescence (panels C), and excitation at 488.0 and 543.5 nm with observation of both fluorescein and rhodamine fluorescence (panels D). Representative optical slices in the middle of the particles were selected.

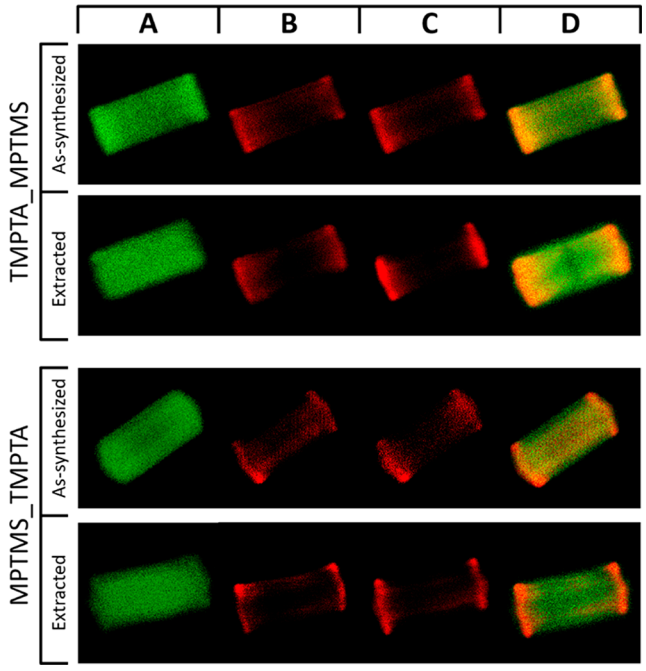

Figure 6. CLSM images of ASNCs prepared by tandem postcondensation. Top: TMPTA and subsequent addition of MPTMS. Bottom: MPTMS and subsequent addition of TMPTA. Excitation at 488.0 nm and observation of fluorescein fluorescence (panels A), excitation at 543.5 nm and observation of rhodamine fluorescence (panels B), excitation at 488.0 nm and observation of rhodamine fluorescence (panels C), and excitation at 488.0 and 543.5 nm with observation of both fluorescein and rhodamine fluorescence (panels D). Representative optical slices in the middle of the particles were selected.

to thiol groups) and panels B for MPTMS_APTMS (rhodamine coupled to amino groups). Panels C of Figure 5 show the results obtained upon irradiating the samples with the fluorescein excitation wavelength (488.0 nm) and observing in the rhodamine fluorescence range. The fluorescent areas represent the energy transfer between fluorescein and rhodamine, indicating regions in the particles where both fluorescent labels, and therefore thiol and amino groups, are present. To obtain a general view of the differently functionalized surfaces, CLSM images with both excitation wavelengths and both observation ranges were acquired and the results are reported in panels D. In these images, the yellow-orange color is due to the overlapping fluorescein and rhodamine emission. This bifunctionalized area indicates that the second silane penetrates to a certain degree into the nanochannels and reacts with the available silanol groups. This is particularly well visible in the image of as-synthesized MPTMS_APTMS, where the differently colored areas are clearly separated.

Tandem Postcondensation with Mixed Bulky and Nonbulky Silanes (Cases I and II). The results of tandem postcondensation with silanes having different degrees of steric hindrance are reported in Figure 6. Classification according to the synthetic strategies shown in Figure 4 depends on the addition sequence. In experiments where the bulky aminosilane TMPTA was added before the nonbulky MPTMS, TMPTA accumulated at the pore entrances according to case II (Figure 6, top, panels B). Panels A in Figure 6 show that the subsequently added MPTMS produced a uniform functionalization with thiol groups. This indicates that the internal surface remains accessible even after functionalization of the pore entrances with TMPTA. Similar results were obtained upon changing the sequence of silane addition (Figure 6, bottom); that is, the amino groups are located at the pore entrances, while the thiol groups mainly occupy pore surface sites. Note that the addition of MPTMS followed by TMPTA corresponds to case I: the initially added MPTMS produced a uniform distribution, whereas the subsequently added TMPTA functionalized the pore entrances.

Tandem Postcondensation with Bulky Silanes (Case II). To obtain more information about the accessibility of the nanochannels, A-Fluo and A-Rhod were used in a tandem postcondensation reaction. The CLSM images of the bifunctionalized products are reported in Figure 7. The first dye silane condensed preferentially at the pore entrances, while the subsequently added dye silane reacted with the nonfunctionalized pore surface. These results establish that the bulky silanes located at the nanochannel entrances are not a limiting factor for further internal functionalization. It can be assumed that, during the addition of the first silane, silicate residues in the reaction mixture assist end-on growth because of the ongoing condensation and cross-linking. Therefore, the first dye silane preferentially accumulates at the pore entrances. The question remains why the second dye silane is able to react with pore surface sites to create a seemingly uniform distribution despite being bulky. Reaction at the pore entrances requires silane cross-linking and a sufficient amount of small residual silicate species to promote end-on growth. At the time of the addition of the second silane, end-on growth has slowed

DOI: 10.1021/acs.chemmater.8b03603
Chem. Mater. 2018, 30, 7280−7286

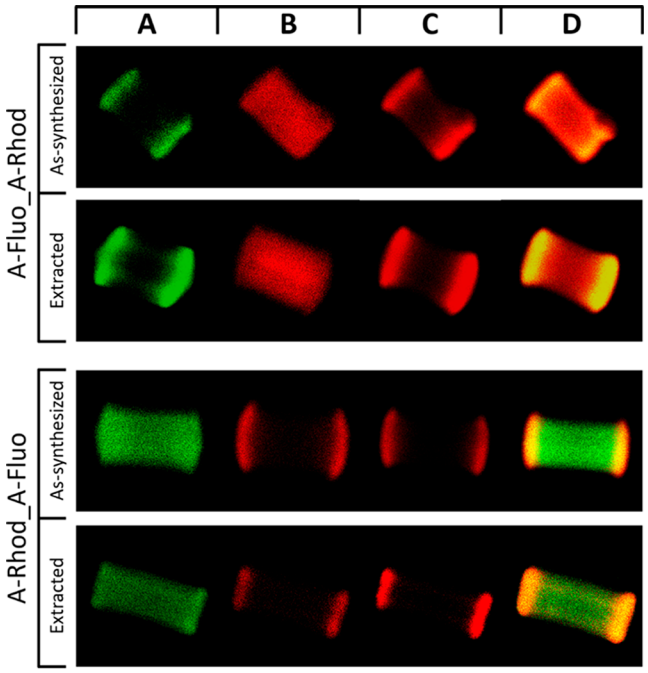

Figure 7. CLSM images of ASNCs prepared by tandem postcondensation. Top: A-Fluo and subsequent addition of A-Rhod. Bottom: A-Rhod and subsequent addition of A-Fluo. Excitation at 488.0 nm and observation of fluorescein fluorescence (panels A), excitation at 543.5 nm and observation of rhodamine fluorescence (panels B), excitation at 488.0 nm and observation of rhodamine fluorescence (panels C), and excitation at 488.0 and 543.5 nm with observation of both fluorescein and rhodamine fluorescence (panels D). Representative optical slices in the middle of the particles were selected.

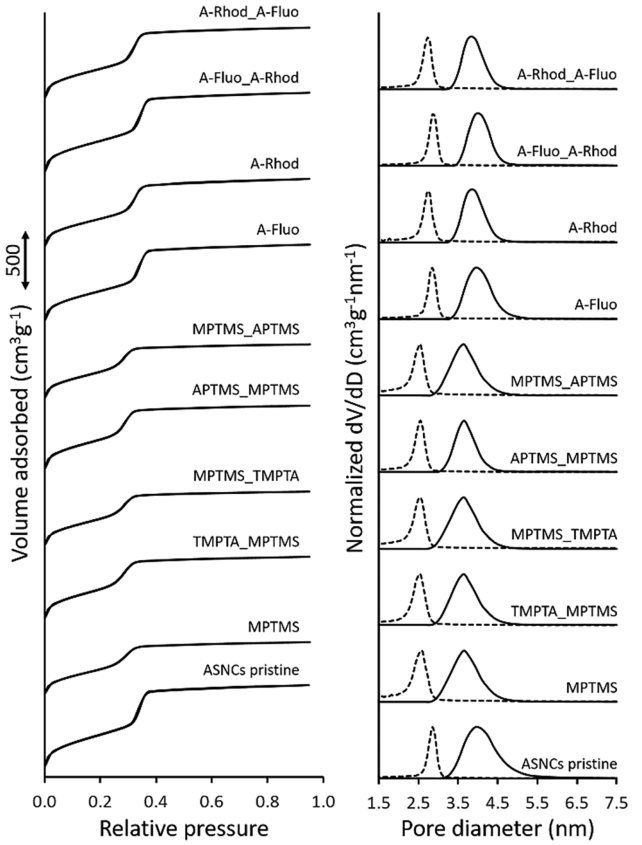

Figure 8. Left: nitrogen sorption isotherms. Right: corresponding pore size distributions (normalized to the same height) obtained with the BJH method (dotted lines) and with the NLDFT method (solid lines). Data of a pristine sample of ASNCs (prepared without the addition of functional silanes) are shown for comparison.

down because of the depletion of the residual silicate species. Furthermore, dye silane cross-linking is comparatively inefficient because of steric hindrance. Combining these effects with the abundance of silanol groups on the yet non-functionalized internal surface ultimately leads to the reaction of the second dye silane with the pore surface silanols.

Porous Properties. Postcondensation and tandem post-condensation methods generally do not cause a significant variation of the porosity compared to a pristine material prepared without the addition of functional silanes.[19] Figure 8 reports the nitrogen sorption isotherms of extracted samples and the respective pore size distributions (PSD) calculated with the BJH and NLDFT methods.[26] The textural properties of the functionalized ASNCs are summarized in Table 1. The reversible Type IVb isotherms are characteristic of ASNCs.[24] The pore condensation step typically occurs at a relative pressure (p/p_0) between 0.27 and 0.37. It should be noted in this context that the NLDFT method uses a kernel that is not strictly valid for organo-functionalized silica surfaces, whereas the BJH method generally underestimates the absolute pore size values when the mesopores are smaller than 10 nm.[26] Irrespective of the method used for calculating the PSD, the properties of the functionalized ASNCs (including BET surface area and pore volume) show a slight variation from batch to batch.[19,25,29] For this reason, the pore size differences between ASNCs postcondensed with R-silanes and ASNCs postcondensed with dye silanes can be attributed partially to the lower dye silane/TEOS ratio employed in the tandem postcondensation with dye silanes. Furthermore, the lower pore volume of

Table 1. Textural Properties of Extracted Samples (Average Pore Diameter Calculated by NLDFT (d_{NLDFT}) and BJH (d_{BJH}), Total Pore Volume (V_{tot}), BET Surface Area (S_{BET}))

	d_{NLDFT} (nm)	d_{BJH} (nm)	V_{tot} ($cm^3 g^{-1}$)	S_{BET} ($m^2 g^{-1}$)
ASNCs pristine	3.9	2.8	1.15	1325
MPTMS	3.7	2.5	0.76	1042
TMPTA_MPTMS	3.7	2.5	0.91	1230
MPTMS_TMPTA	3.7	2.5	0.80	1120
APTMS_MPTMS	3.7	2.5	0.95	1093
MPTMS_APTMS	3.7	2.5	0.79	1285
A-Fluo	3.9	2.8	1.11	1270
A-Rhod	3.9	2.7	1.00	1212
A-Fluo_A-Rhod	3.9	2.8	1.16	1335
A-Rhod_A-Fluo	3.8	2.7	1.05	1277

the samples prepared with MPTMS or with MPTMS as the first added silane is indicative of the high degree of pore surface functionalization with thiol groups.

The large surface area and the large pore volume of multifunctionalized ASNCs are evidence that the particles preserve their characteristic mesoporosity after the tandem postcondensation process. During the formation of the ASNCs, the structure-directing agent promotes the silica growth, creating an ordered mesoporous system.[29−31] After the first addition (postcondensation) the functional silanes condense uniformly on the surfaces (case I) or continue to

DOI: 10.1021/acs.chemmater.8b03603
Chem. Mater. 2018, 30, 7280−7286

build the framework, particularly at the pore entrances via end-on growth (case II). The structure-directing agent limits the efficient migration of the silanes into the channels, but it still allows the formation of a functional pore surface layer, thereby slightly decreasing the pore diameter (Figure 8). On the external surface, in particular at the nanochannel entrances, the functional silane and the silicate residues condense around the structure-directing agent. This creates an organo-functionalized ordered framework similar to the framework obtained in a conventional co-condensation process[15,16] and in agreement with the reversible nitrogen sorption isotherms. Any subsequently added silane reacts with the available silanol groups. These sites are mainly located at the pore entrances if the pore surface is already functionalized to a high degree (case I) or on the pore surface if the entrances have been functionalized during the first step of the tandem post-condensation (case II).

CONCLUSIONS

Postcondensation is a novel pathway to synthesize functional mesoporous silica particles through a one-pot reaction. The steric hindrance and the mobility of the functional silanes, supported by the end-on particle growth, were used as driving forces to functionalize the different surface regions of ASNCs. To achieve multifunctionalized particles, a one-pot tandem postcondensation method was developed. The nanochannel entrances and the internal surfaces were selectively functionalized with amino and thiol groups, preserving the characteristic mesoporosity and hexagonal prismatic morphology of the ASNCs. The selective customization of different particle surface regions opens possibilities for the creation of a versatile platform. Applications based on the coupling of the surface-bound functional groups with active molecules can be envisaged.[32] Stimuli-responsive gates[7,9,33,34] or target anchoring sites[18,33,35] can be selectively attached to the pore entrances. The pore surface can be customized independently to increase the capacity for storing guest species, to promote catalytic reactions, or to selectively detect a target substance.

ASSOCIATED CONTENT

Supporting Information

The Supporting Information is available free of charge on the ACS Publications website at DOI: 10.1021/acs.chemmater.8b03603.

> Non-normalized pore size distributions, comparison of BET surface area and external surface area, CLSM images at various *z*-axis positions, evaluation of functional silane contents, and role of excess APTMS in the postcondensation of A-Fluo and A-Rhod (PDF)

AUTHOR INFORMATION

Corresponding Author

*E-mail: dominik.bruehwiler@zhaw.ch.

ORCID

Dominik Brühwiler: 0000-0002-9284-5144

Author Contributions

The manuscript was written through contributions of all authors. All authors have given approval to the final version of the manuscript.

Funding

This work was supported by the Swiss National Science Foundation (project 200021_172805).

Notes

The authors declare no competing financial interest.

REFERENCES

(1) Beck, J. S.; Vartuli, J. C.; Roth, W. J.; Leonowicz, M. E.; Kresge, C. T.; Schmitt, K. D.; Chu, C. T.-W.; Olson, D. H.; Sheppard, E. W.; McCullen, S. B.; Higgins, J. B.; Schlenker, J. L. A New Family of Mesoporous Molecular Sieves Prepared with Liquid Crystal Templates. *J. Am. Chem. Soc.* **1992**, *114*, 10834−10843.

(2) Huang, X.; Li, L.; Liu, T.; Hao, N.; Liu, H.; Chen, D.; Tang, F. The Shape Effect of Mesoporous Silica Nanoparticles on Biodistribution, Clearance, and Biocompatibility in Vivo. *ACS Nano* **2011**, *5*, 5390−5399.

(3) Travaglini, L.; De Cola, L. Morphology Control of Mesoporous Silica Particles Using Bile Acids as Co-Surfactants. *Chem. Mater.* **2018**, *30*, 4168−4175.

(4) Brühwiler, D. Postsynthetic Functionalization of Mesoporous Silica. *Nanoscale* **2010**, *2*, 887−892.

(5) Duan, R.; Xia, F.; Jiang, L. Constructing Tunable Nanopores and Their Application in Drug Delivery. *ACS Nano* **2013**, *7*, 8344−8349.

(6) Maggini, L.; Cabrera, I.; Ruiz-Carretero, A.; Prasetyanto, E. A.; Robinet, E.; De Cola, L. Breakable Mesoporous Silica Nanoparticles for Targeted Drug Delivery. *Nanoscale* **2016**, *8*, 7240−7247.

(7) Giret, S.; Wong Chi Man, M.; Carcel, C. Mesoporous-Silica-Functionalized Nanoparticles for Drug Delivery. *Chem. - Eur. J.* **2015**, *21*, 13850−13865.

(8) Mbaraka, I. K.; Shanks, B. H. Design of Multifunctionalized Mesoporous Silicas for Esterification of Fatty Acid. *J. Catal.* **2005**, *229*, 365−373.

(9) Castillo, R. R.; Baeza, A.; Vallet-Regí, M. Recent Applications of the Combination of Mesoporous Silica Nanoparticles with Nucleic Acids: Development of Bioresponsive Devices, Carriers and Sensors. *Biomater. Sci.* **2017**, *5*, 353−377.

(10) El-Safty, S. A.; Abdellatef, S.; Ismael, M.; Shahat, A. Optical Nanosphere Sensor Based on Shell-by-Shell Fabrication for Removal of Toxic Metals from Human Blood. *Adv. Healthcare Mater.* **2013**, *2*, 854−862.

(11) Sun, Z.; Cui, G.; Li, H.; Liu, Y.; Tian, Y.; Yan, S. Multifunctional Optical Sensing Probes Based on Organic-Inorganic Hybrid Composites. *J. Mater. Chem. B* **2016**, *4*, 5194−5216.

(12) Da'na, E. Adsorption of Heavy Metals on Functionalized-Mesoporous Silica: A Review. *Microporous Mesoporous Mater.* **2017**, *247*, 145−157.

(13) Salis, A.; Medda, L.; Cugia, F.; Monduzzi, M. Effect of Electrolytes on Proteins Physisorption on Ordered Mesoporous Silica Materials. *Colloids Surf., B* **2016**, *137*, 77−90.

(14) Silva, M.; Pérez-Quintanilla, D.; Morante-Zarcero, S.; Sierra, I.; Marina, M. L.; Aturki, Z.; Fanali, S. Ordered Mesoporous Silica Functionalized with *β*-Cyclodextrin Derivative for Stereoisomer Separation of Flavanones and Flavanone Glycosides by Nano-Liquid Chromatography and Capillary Electrochromatography. *J. Chromatogr. A* **2017**, *1490*, 166−176.

(15) Vinu, A.; Hossain, K. Z.; Ariga, K. Recent Advances in Functionalization of Mesoporous Silica. *J. Nanosci. Nanotechnol.* **2005**, *5*, 347−371.

(16) Hoffmann, F.; Cornelius, M.; Morell, J.; Fröba, M. Silica-Based Mesoporous Organic-Inorganic Hybrid Materials. *Angew. Chem., Int. Ed.* **2006**, *45*, 3216−3251.

(17) Bois, L.; Bonhommé, A.; Ribes, A.; Pais, B.; Raffin, G.; Tessier, F. Functionalized Silica for Heavy Metal Ions Adsorption. *Colloids Surf., A* **2003**, *221*, 221−230.

(18) Möller, K.; Bein, T. Talented Mesoporous Silica Nanoparticles. *Chem. Mater.* **2017**, *29*, 371−388.

DOI: 10.1021/acs.chemmater.8b03603
Chem. Mater. 2018, 30, 7280−7286

(19) Zucchetto, N.; Brühwiler, D. Functionalization of Arrays of Silica Nanochannels by Post-Condensation. *Dalton Trans.* **2016**, *45*, 14363−14369.
(20) Ban, T.; Brühwiler, D.; Calzaferri, G. Selective Modification of the Channel Entrances of Zeolite L with Triethoxysilylated Coumarin. *J. Phys. Chem. B* **2004**, *108*, 16348−16352.
(21) Tabacchi, G.; Fois, E.; Calzaferri, G. Structure of Nanochannel Entrances in Stopcock-Functionalized Zeolite L Composites. *Angew. Chem., Int. Ed.* **2015**, *54*, 11112−11116.
(22) Calzaferri, G.; Huber, S.; Maas, H.; Minkowski, C. Host-Guest Antenna Materials. *Angew. Chem., Int. Ed.* **2003**, *42*, 3732−3758.
(23) Cao, P.; Khorev, O.; Devaux, A.; Sägesser, L.; Kunzmann, A.; Ecker, A.; Häner, R.; Brühwiler, D.; Calzaferri, G.; Belser, P. Supramolecular Organization of Dye Molecules in Zeolite L Channels: Synthesis, Properties, and Composite Materials. *Chem. - Eur. J.* **2016**, *22*, 4046−4060.
(24) Zucchetto, N.; Brühwiler, D. Tuning the Aspect Ratio of Arrays of Silica Nanochannels. *RSC Adv.* **2015**, *5*, 74638−74644.
(25) Gartmann, N.; Brühwiler, D. Controlling and Imaging the Functional-Group Distribution on Mesoporous Silica. *Angew. Chem., Int. Ed.* **2009**, *48*, 6354−6356.
(26) Thommes, M.; Kaneko, K.; Neimark, A. V.; Olivier, J. P.; Rodriguez-Reinoso, F.; Rouquerol, J.; Sing, K. S. W. Physisorption of Gases, with Special Reference to the Evaluation of Surface Area and Pore Size Distribution (IUPAC Technical Report). *Pure Appl. Chem.* **2015**, *87*, 1051−1069.
(27) Neimark, A. V.; Ravikovitch, P. I. Capillary Condensation in MMS and Pore Structure Characterization. *Microporous Mesoporous Mater.* **2001**, *44*−*45*, 697−707.
(28) Brunauer, S.; Emmett, P. H.; Teller, E. Adsorption of Gases in Multimolecular Layers. *J. Am. Chem. Soc.* **1938**, *60*, 309−319.
(29) Kievsky, Y.; Sokolov, I. Self-Assembly of Uniform Nanoporous Silica Fibers. *IEEE Trans. Nanotechnol.* **2005**, *4*, 490−494.
(30) Yang, H.; Coombs, N.; Ozin, G. A. Morphogenesis of Shapes and Surface Patterns in Mesoporous Silica. *Nature* **1997**, *386*, 692−695.
(31) Ozin, G. A.; Kresge, C. T.; Yang, H. Nucleation, Growth and Form of Mesoporous Silica: Role of Defects and a Language of Shape. *Stud. Surf. Sci. Catal.* **1998**, *117*, 119−127.
(32) Chiu, H. Y.; Gößl, D.; Haddick, L.; Engelke, H.; Bein, T. Clickable Multifunctional Large-Pore Mesoporous Silica Nanoparticles as Nanocarriers. *Chem. Mater.* **2018**, *30*, 644−654.
(33) Yang, P.; Gai, S.; Lin, J. Functionalized Mesoporous Silica Materials for Controlled Drug Delivery. *Chem. Soc. Rev.* **2012**, *41*, 3679−3698.
(34) Sancenón, F.; Pascual, L.; Oroval, M.; Aznar, E.; Martínez-Máñez, R. Gated Silica Mesoporous Materials in Sensing Applications. *ChemistryOpen* **2015**, *4*, 418−437.
(35) Cheng, S.-H.; Lee, C.-H.; Chen, M.-C.; Souris, J. S.; Tseng, F.-G.; Yang, C.-S.; Mou, C.-Y.; Chen, C.-T.; Lo, L.-W. Tri-Functionalization of Mesoporous Silica Nanoparticles for Comprehensive Cancer Theranostics The Trio of Imaging, Targeting and Therapy. *J. Mater. Chem.* **2010**, *20*, 6149−6157.

DOI: 10.1021/acs.chemmater.8b03603
Chem. Mater. 2018, 30, 7280−7286